ADVANCED ELECTRONIC MATERIALS Open Access
www.advelectronicmat.de

Inkjet Printed Multifunctional Graphene Sensors for Flexible and Wearable Electronics

Feiran Wang, Charles E. D. Heaton, Nathan D. Cottam, Jonathan S. Austin, Jisun Im, T. Mark Fromhold, Ricky D. Wildman, Richard J. M. Hague, Christopher J. Tuck, Oleg Makarovsky, and Lyudmila Turyanska**

The exceptional electrical properties of graphene with high sensitivity to external stimuli make it an ideal candidate for advanced sensing technologies. Inkjet printing of graphene (iGr) can provide a versatile platform for multifunctional sensor manufacturing. Here the multifunctional sensor enabled by combining the design freedom of inkjet printing with the unique properties of graphene networks is reported on. A fully inkjet printed multimaterial device consists of two layers of iGr stripes separated by a dielectric polymeric layer of tripropylene glycol diacrylate (TPGDA). In these devices, the bottom iGr layer, capped with TPGDA, provides temperature sensing, the top uncapped iGr is sensitive to the external atmosphere, while the capacitance between the two iGr layers is sensitive to the applied pressure. The fast, sensitive, and reproducible performance of these sensors are demonstrated in response to environmental stimuli, such as pressure, temperature, humidity, and magnetic field. The devices are capable of simultaneous sensing of multiple factors and are successfully manufactured on a variety of substrates, including Si/SiO_2, flexible Kapton films and textiles, demonstrating their potential impact in applications compatible with silicon technologies as well as wearable and healthcare devices.

1. Introduction

Development and implementation of multifunctional sensors and fixed sensor network infrastructures require flexible, non-toxic, and highly sensitive devices, which could bring transformative solutions for applications ranging from healthcare[1] to environmental monitoring.[2] The sensitivity of the electrical properties of exfoliated single layer graphene to the presence of nearby charges[3] has been exploited in photon sensing,[4,5] temperature, pressure,[6] gas,[7] electric field[3] and magnetic field[8] sensors, highlighting their applicability across a range of important measurements. However, the manufacturing scalability of graphene devices is difficult to achieve. Additive manufacturing offers potential solutions, with liquid exfoliation of graphene flakes enabling the formulation of printable inks.[9] In particular, inkjet printing graphene (iGr) offers a route toward large scale device fabrication with a high degree of geometrical design freedom and compatibility with various substrates, including flexible[10] and biocompatible[11] materials. By exploiting the inherent ability of inkjet printing that allows the contemporaneous co-deposition of other functional materials, inkjet deposition could also be used to enable the integration of multiple functionalities within a single structure. This offers opportunities to control device performance by both material and geometry selection.

In iGr networks the electrical properties are defined by the sensitivity of individual flakes to the presence of nearby charges and the contribution of charge transport affected by the flake packing.[12–15] The arrangement of the graphene flakes within the printed film is controlled by the deposition parameters,[16] alongside post-processing techniques.[17] The uniformity of the printed layers, which can be affected by phenomena such as the coffee-ring effect,[12,18,19] as well as the screening of the local electric fields in multi-flake devices,[20] can affect the sensitivity of the sensors.

We report on a fully inkjet printed multifunctional iGr sensor, responsive to a range of external stimuli (e.g., temperature, pressure, humidity, and magnetic fields), and suitable for deployment

F. Wang, C. E. D. Heaton, J. S. Austin, J. Im[+], R. D. Wildman, R. J. M. Hague, C. J. Tuck, L. Turyanska
Centre for Additive Manufacturing
Faculty of Engineering
University of Nottingham
Nottingham NG7 2RD, UK
E-mail: F.Wang@nottingham.ac.uk; Lyudmila.Turyanska@nottingham.ac.uk

N. D. Cottam, T. M. Fromhold, O. Makarovsky
School of Physics and Astronomy
University of Nottingham
Nottingham NG7 2RD, UK

The ORCID identification number(s) for the author(s) of this article can be found under https://doi.org/10.1002/aelm.202400689

[+]Present address: School of Engineering, University of Warwick, Coventry CV4 7AL, UK

DOI: 10.1002/aelm.202400689

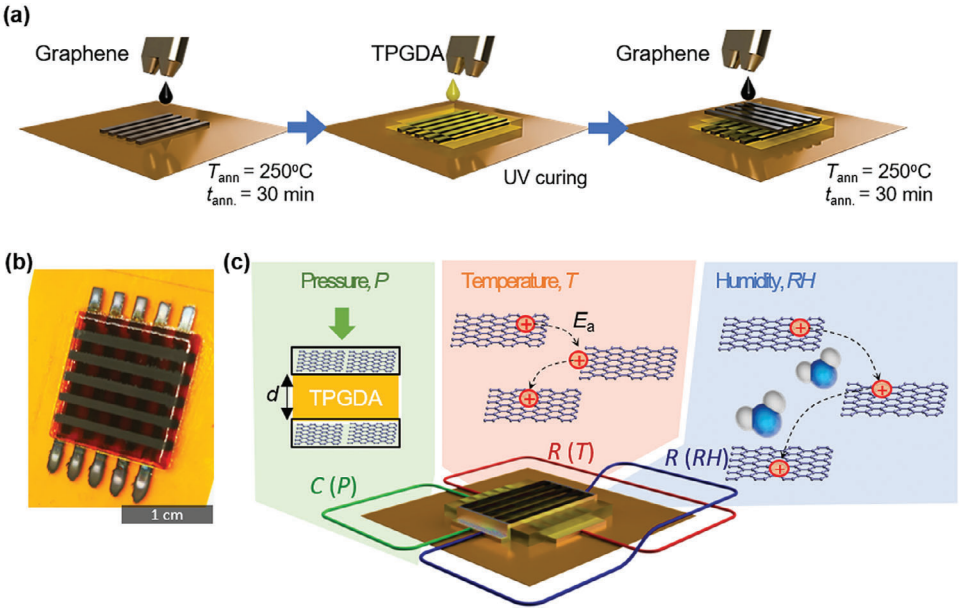

Figure 1. a) Schematic illustration of inkjet printing of graphene (iGr) and polymeric layer (TPGDA) into a multifunctional sensor design and b) a photograph of the sensor. c) A diagram of the electrical circuit and corresponding cartoons illustrating the response of the sensor to (from left to right) pressure, *P*, temperature, *T*, and relative humidity, *RH*.

within silicon-based as well as flexible and wearable electronics. We utilize the design freedom offered by inkjet deposition to manufacture a fully inkjet-printed multimaterial device consisting of two layers of iGr stripes separated by a dielectric polymeric layer of tripropylene glycol diacrylate (TPGDA). In these devices, the bottom iGr layer is capped with TPGDA and provides temperature sensing, and only the top uncapped iGr is sensitive to the external atmosphere. The presence of TPGDA layer between the two iGr layers enables capacitive sensing of applied pressure. The geometry of the device, combined with fundamental understanding of the electrical properties of graphene networks formed in iGr enable us to realize independent and simultaneous sensing of multiple stimuli. A phenomenological model has been proposed to explain the mechanism of sensing in these devices. Successful demonstration of a multifunctional iGr sensor manufactured onto a number of substrates from solid (Si/SiO_2) to flexible (Kapton film and textiles) could provide a platform for the development of future iGr-based devices with multifunctional sensing capabilities for applications from healthcare to environmental monitoring.

2. Results and Discussion

We designed and fabricated a graphene-based multifunctional sensor using multimaterial, multilayer inkjet printing technology (**Figure** 1a,b). In this design, devices consisting of two iGr layers separated by an insulating layer of tripropylene glycol diacrylate (TPGDA) were printed onto a flexible Kapton substrate, forming iGr/TPGDA/iGr heterostructure. The top and bottom iGr layers were printed perpendicular with respect to each other and consisted of five independent parallel stripes with sizes of 0.12 cm × 1.20 cm separated by 0.15 cm. The overall size of the device is 1.2 cm × 1.2 cm. TPGDA was selected as the separating dielectric material due to its balance of dielectric and mechanical properties, thermal stability, and reliable performance in inkjet printing.[21]

Electrical contacts were printed with the Ag-nanoparticle ink and were used to allow independent measurements of the lateral resistance of the top and bottom iGr stripes as well as the vertical capacitance between the iGr layers. The device was designed to enable simultaneous sensing of the three external stimuli: the bottom iGr layer is used for temperature (*T*) sensing, the top iGr is used for relative humidity (*RH*) sensing and the vertical capacitance of the iGr/TPGDA/iGr heterostructure is used for pressure (*P*) sensing, providing a proof-of-concept of the technology (Figure 1c). In this sensor architecture, the electrical conduction of graphene networks in iGr is highly temperature dependent, allowing *T*-sensing through measurements of resistance change, *R*(*T*). The top layer of graphene is exposed to the atmosphere, enabling environmental (e.g., humidity, gas) sensing, *R*(*RH*). The electrical resistance between the top and bottom graphene layers is affected by the thickness change of the separating dielectric layer (TPGDA) in response to compression, hence enabling *P*-sensing, *C*(*P*).

The temperature dependence of the electrical properties is also affected by the iGr layer thickness. Our previous Monte Carlo simulations[12] demonstrated that flake packing density defines the electrical properties of iGr, and it reaches its saturation for films printed with multiple layers. The electrical conductivity $\sigma(T)$ of the devices with the total number of printed layers $N_L > 5$ (**Figure** 2a) showed the temperature dependence characteristic expected for a 3D variable range hopping mechanism:

$$\sigma(T) \propto \exp\left[-\left(\frac{T_0}{T}\right)^p\right] \quad (1)$$

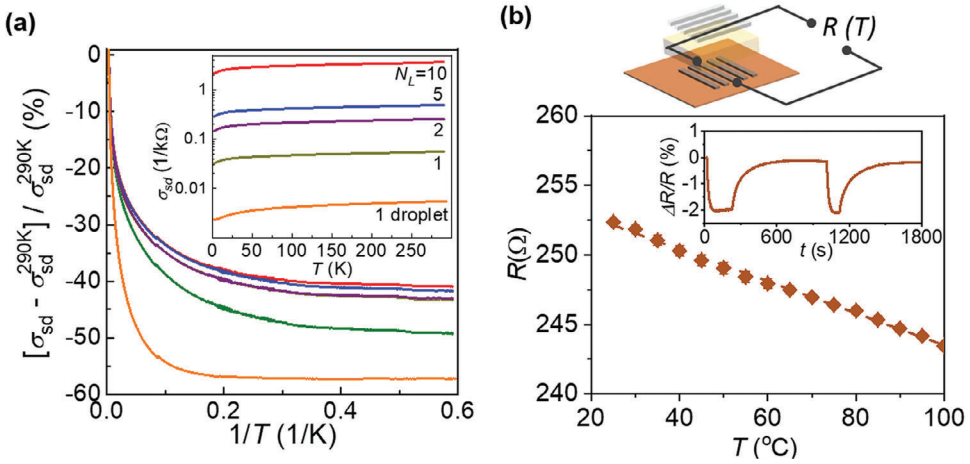

Figure 2. a) Temperature dependence of the normalized conductivity (relative to conductivity at room temperature, $T = 290$ K) and 2D conductivity (inset) for iGr devices with different thickness (N_L is the number of printed layers). b) Temperature dependence of the resistance of bottom iGr stripes of the sensor during two heating/cooling cycles in the temperature 25 °C < T < 80 °C. Inset: temporal response of the temperature sensor at $T = 60$ °C.

where T_0 is a characteristic temperature and $p = 1/4$. However, a large uncertainty of the $\sigma(T)$ is observed for the droplet devices, likely due to increased variability of the formation of conductive graphene networks and increased contribution of intra-flake transport.[12] For all samples with the number of printed layers $N_L \geq 5$ the $\sigma(T)$ is comparable (Figure 2a), hence the activation energy of thermally induced charge transport is the same and the T-sensing performance is independent of N_L making them suitable for device applications.

In our sensor design, the conductivity of the bottom iGr layer is only affected by the sample temperature, as it is capped with the dielectric layer which provides we protection from the environment. The five iGr stripes with $N_L = 10$ connected in parallel (Figure 1b) have a total resistance of ≈250 Ω. With increasing temperature from $T = 25$ to 80 °C, the resistance changes by 4.5% (Figure 2b) and this change can be fitted with Arrhenius equation $R \propto \exp(E_a/k_B T)$ with an activation energy $E_a = 1.8$ meV. The response to T is fully reversible (inset in Figure 2b) and has ON/OFF times of $t_{on}(T)$ ≈30 s and $t_{off}(T) > 200$ s for an ambient temperature of $T = 60$ °C.

The top iGr layer is uncapped and exposed to the atmosphere, making it suitable for environmental sensing. In response to 100% relative humidity (RH), the resistance of iGr increases by 2.5%. The temporal response is fully reversible over at least ten cycles (Figure 4a) with response times of $t_{on}(RH)$ ≈1 s and $t_{off}(RH) = 5$ s for 2 s exposure to 100% RH. Exposure to humidity can lead to the adsorption of water molecules into the iGr layer, causing an increase in the inter-flake distance.[22] The change of resistance in response to different levels of RH can be fitted with $R \propto 1/d_{eff}$, where d_{eff} is an effective thickness of iGr following the adsorption of water molecules (**Figure 3a**). Under prolonged exposure (at least 30 min) to constant levels of RH, the response remains stable, while under exposure to continuously increasing humidity, the resistance is continuously increasing (Figure S1a, Supporting Information). Note that exposure to humidity has no impact on the resistance of the bottom iGr layer and therefore does not affect T-sensing, allowing for T and humidity sensing to be performed simultaneously and independently.

The additive nature of the inkjet printing and the high degree of design freedom enabled us to integrate additional sensing capabilities. For example, the humidity sensing capability of iGr can be potentially used indirectly to monitor drug release. To demonstrate this, we inkjet-printed a water-soluble layer of 4-acryloylmorpholine[23] loaded with temozolomide (TMZ-ACMO) (Figure S1b, Supporting Information) on top of the sensor. When exposed to water, ACMO dissolves releasing TMZ. The dissolution of the TMZ-ACMO layer leads to exposure of the top iGr layer to water, resulting in the resistance increase of the iGr layer by up to 12.3% for fully dissolved TMZ-ACMO layer.

The sensor can also be used to monitor pressure by measuring the capacitance change of the matrix of 25 iGr/TPGDA/iGr parallel plate capacitors (Figure 1). The capacitance of the device is

$$C = \frac{\varepsilon_r \varepsilon_0 A}{d(P)} \quad (2)$$

where $\varepsilon_r = 3.03$ is the relative dielectric constant of TPGDA, $A = 36$ mm^2 is the total area, and $d(P)$ is the thickness of the TPGDA layer when the pressure P is applied. The applied pressure compresses the TPGDA dielectric layer, changing the distance, $d(P)$, between the iGr layers that act as bottom and top plates of the capacitor. The $d(P)$ can be estimated by the following equation, $d(P) = d_0 (1 - P/E)$, where $d_0 = 410$ µm is the thickness of TPGDA under zero pressure, and $E = 2.5 \times 10^5$ N m^{-2} is the Young's modulus of TPGDA.[21] The capacitance of the device increases linearly from 2.5 to 2.8 pF in response to the applied pressure from 0 to 10 kPa (Figure 3b; Figure S1c, Supporting Information). The response is fully reversible with pressure independent response times of $t_{on}(P)$ ≈0.5 s and $t_{off}(P) = 2$ s. Equation (2) provides a good fit to the experimental data (Figure 3b) and could be used to guide the material choice and design options for other printed pressure sensors. The performance of the mul-

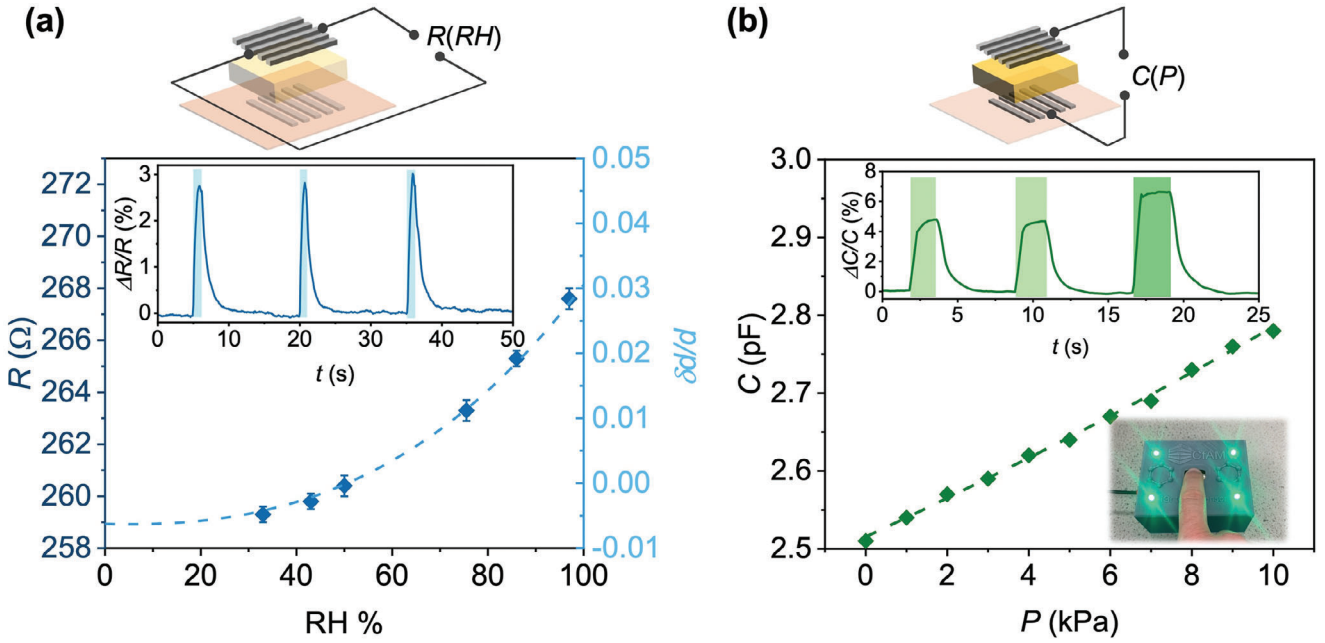

Figure 3. a) Dependence of iGr resistance on the relative humidity (*RH*) of the environment and (Inset) temporal response of iGr-humidity sensor in response to *RH* = 100%. Dashed line represents the calculated $R \propto 1/d_{eff}$ dependence. b) Change of capacitance for the iGr-TPGDA-iGr sandwich structure in response to applied pressure. The dashed line represents a fit to the Equation (2). Inset: Temporal response of the device to the repeated cycles of applied pressure between 4 and 7 kPa and photograph of iGr touch sensor, where proximity to a human finger causes a signal change in the printed flakes and stimulates LED illumination.

tilayer, multifunctional iGr sensor is reproducible and stable over at least 100 cycles of exposure to temperature, humidity and pressure. We note that the sensitivity of inter-flake charge transport[24] in graphene networks to the applied external fields can be exploited for magnetic field sensing. In the iGr_{film} devices with $N_L >$ 4, the magnetoresistance increases linearly with increasing magnetic fields, $B >$ 5T (Figure S2, Supporting Information),[25–28] demonstrating high sensitivity magnetic field detection.

Under simultaneous exposure to multiple stimuli, the individual responses were successfully extracted. For example, since in the device design, the bottom iGr layer is capped with TPGDA, it is only sensitive to *T* and not to *RH*. Under simultaneous exposure, the *T*-response of the bottom iGr layer can be subtracted from the response of the top layer, providing an *RH* sensing value. The capacitance change due to the applied pressure is also consistent under different temperatures. To illustrate the simultaneous sensing capabilities, we tested our device under different temperatures $T = 30$, 40 and 50 °C with a simultaneous humidity stimulation ($RH \approx 100\%$) and under applied pressure ($P \approx 2$ kPa), and observed distinguishable and reproducible response (Figure S1d, Supporting Information).

The sensing modalities demonstrated here for the iGr devices offer exciting multifunctionality for numerous sensing applications. Compatibility of inkjet deposition process with a variety of substrates could provide solutions for integrating sensors with existing facilities and devices as well as for wearable and flexible electronics. To achieve controlled and reproducible device manufacturing and performance, it is necessary to understand the effect of the deposition process and film morphology on the electrical properties of iGr. A number of samples was examined from single droplets, iGr_{drop}, to films, iGr_{film}, produced with different number of printed layers (from $N_L = 1$ to $N_L = 10$) (**Figure** 4a; Figure S3, Supporting Information). The single droplet devices have the minimum electrical resistivity, corresponding to the Dirac point, at $V_g = 80 \pm 20$ V ($p \approx 5 \times 10^{12}$ cm^{-2}) and relatively low field effect mobility, $\mu \approx 1$ cm^2 V^{-1}s^{-1} (Figure S4, Supporting Information). The 2D sheet resistance of iGr_{drop} devices decreases with increasing N_L from $\rho_{2D} > 50$ kΩ for $N_L = 1$ to $\rho_{2D} \approx 3$ kΩ for $N_L = 5$. For iGr_{film} devices the sheet resistance also decreases with increasing sample thickness. We note, that electrical properties of iGr are reproducible for devices printed on various substrates, including flexible polymeric substrates. For the devices printed on Kapton and on fabric, the iGr_{films} integrity and electrical resistivity remain unchanged after at least 10 000 (Figure 4b) and 1000 bending cycles (Figure S5, Supporting Information), respectively. For example, for the iGr on Kapton undergoing ≈15° bending and for iGr on fabric undergoing ≈30° bending for up to 10 000 and 100 bending cycles, respectively, we observe negligible < 0.2% change of resistance. We note, that this change is significantly smaller compared to response to external stimuli, confirming that these devices can be used for flexible and wearable electronics.

Since the drop spreading on the substrate during deposition is affected by the number of printed layers, we introduced the concept of an effective number of layers, $N_{eff} = N_L A_{des}/A_{mes}$, where A_{des} is the designed area and A_{mes} is the measured area of the printed sample (Figure S3, Supporting Information). The iGr stripes with $N_{eff} \geq 4$ demonstrate the sheet resistance $\rho_{2D} \approx 1/N_{eff}$, typical for a 3D material, while for the samples with $N_{eff} < 4$, the dependence can be fitted with $\rho_{2D} \approx 1/N^2_{eff}$ (Figure 4c).

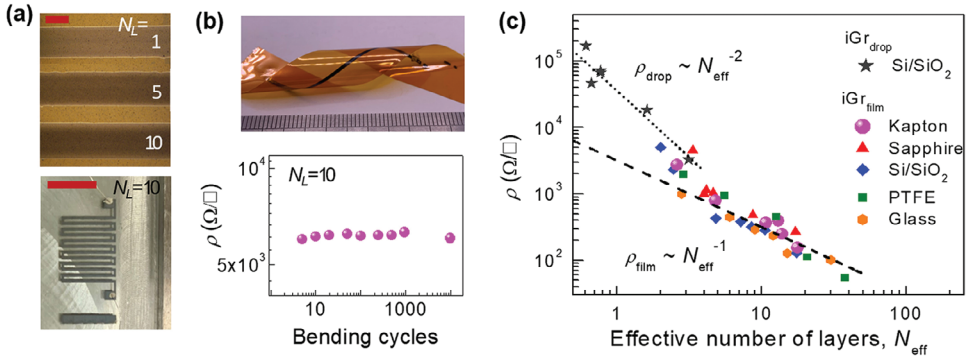

Figure 4. a) Optical images of iGr samples inkjet printed with different numbers of layers, N_L, onto (top) Kapton and (bottom) glass (scale bar 500 µm); b) A photograph of iGr film (N_L = 10) on flexible Kapton substrate and (bottom) an electrical resistivity of the iGr film after up to 10 000 bending cycles. c) Dependence of the sheet resistance of inkjet printed graphene devices on the effective number of layers and fitted dependences (dashed lines).

We attribute the difference between the droplet and film devices to the high contribution of intra-flake (individual flakes) charge transport in droplet devices compared to charge transport being dominated by inter-flake (flake-to-flake) charge transfer.[25]

Note that these dependencies are independent of the substrate used, as demonstrated here for Si/SiO$_2$, sapphire, glass, Kapton, and PTFE substrates, and do not change after capping of iGr films with polymeric materials (e.g., TPGDA). We ascribe this behavior to the contribution of quantum effects, such as flake-to-flake tunnelling and an increasing role of the intra-flake transport to the overall electrical properties of the graphene network.[21]

To demonstrate the potential of this technology for wearable sensors, we demonstrate an iGr sensor printed onto a fabric (**Figure 5**). Prior to inkjet deposition of iGr onto a polyester-cotton a primer layer of TPGDA was deposited onto the fabric fibres to decrease the sinking of graphene inks into the porous fabric. Response to temperature, humidity and pressure of this wearable device is comparable to that demonstrated on Kapton. Temperature dependent resistance measurements were carried out on the iGr fabric device, with the electrical response being measured over the temperature range of 20 °C < T < 95 °C. A $R \propto \exp(1/T)$ relation was exhibited between the device's resistance and local temperature, with a total change up to 22% observed for 95 °C (Figure 5b). The humidity response to a person breathing across the device caused a 3.8% increase of resistance, with a fast response and recovery times of less than 5 s (Figure 5c). We note

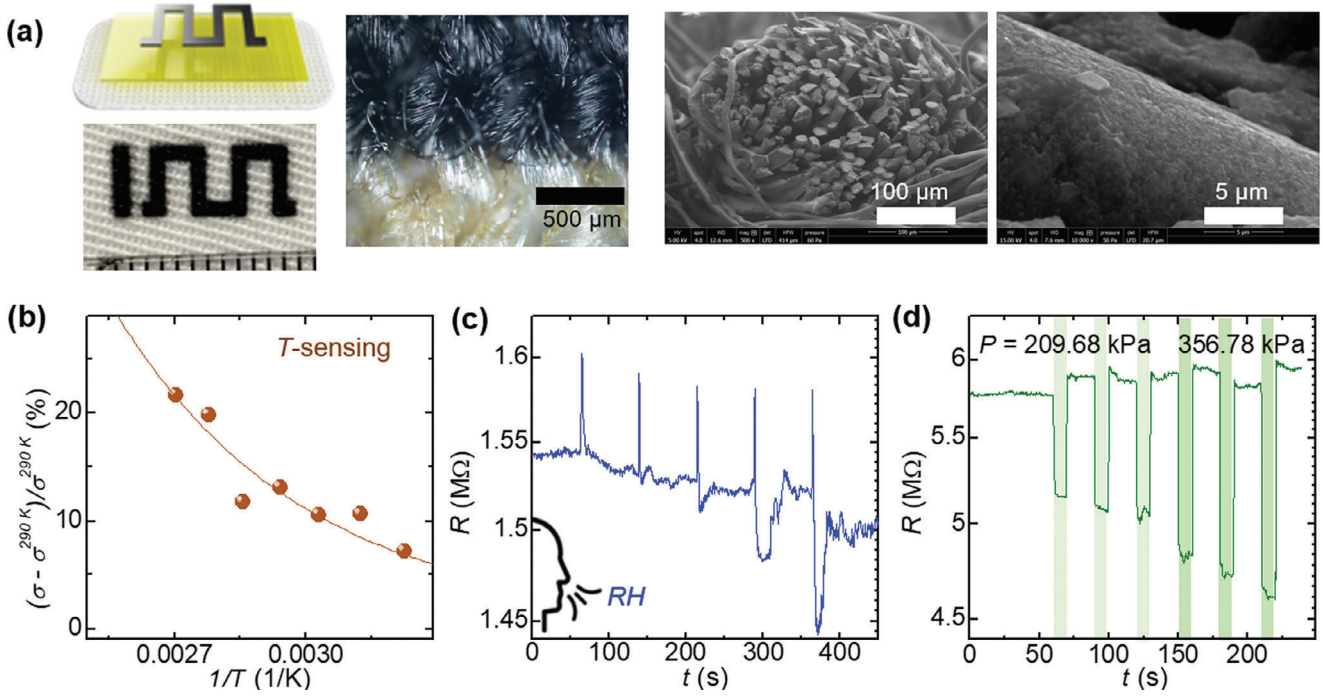

Figure 5. Inkjet printed graphene/TPGDA heterostructures on fabrics. a) Photographs and ESEM images of the cross section and the surface of the fabric fibre. b) Temperature dependence of conductivity for T = 20 to 95 °C. c) Real-time humidity sensing performance of the device on fabrics at RH = 100%. d) Real-time pressure sensor test under different applied pressure.

that the change of T caused by exhaled air is small (< 5 °C) and does not significantly affect the measured values, however this temperature change is likely responsible for the small change in resistance observed after recovery.

On fabric, the distribution of graphene throughout the porous structure of the fibers results in a significantly higher inter-flake spacing (lower packing density of graphene flakes) compared to iGr printed on Kapton or other rigid substrates. With decreasing packing density, the separation between the individual graphene flakes is increasing,[12] hence the resistance of the iGr increases. This offers higher sensitivity for P-sensing, as with applied pressure, the separation between the flakes changes, leading to a change of resistance. When pressure is applied, the fabric is compressed, causing increased flake proximity, thereby resulting in stronger and faster increase of the conductivity, compared to the sensor on Kapton. Thus, on fabrics, pressure can be sensed by the iGr layer alone, without the need for an iGr/TPGDA/iGr sandwich structure and capacitance measurements. The pressure sensing was investigated for two values of pressure, ~210 and ~567 kPa, applied for 10 s, which caused a sharp decrease of the electrical resistance by ≈10% and ≈19c%, respectively (Figure 5d), followed by a fast (≪ 0.5 s) recovery. We note that any change of temperature does not significantly affect this measurement (Figure 5b).

We have demonstrated that the sensitivity of graphene networks to external triggers, combined with opportunities for inkjet-printing design freedom, offers a route for personalized and/or targeted sensing solutions for specific applications. Integration of multiple functionalities in a single sensor provides reliable discrimination of the output responses to each stimulus and offer opportunities for scalable manufacturing. The demonstrated iGr sensor can be fabricated onto conventional Si-based devices to functionalize them with complementary capabilities,[29,30] offering a scalable solution compatible with traditional semiconductor processing. The multifunctionalities, especially the quantum transport natures observed in iGr, will also advance device fabrication options for quantum technologies, offering an integrated and innovative approach for compact and deployable devices, which are currently challenging to achieve. This could pave the way for quantum sensing, timing, computing, etc.[31] In our device architecture, we separate iGr layers that are used for simultaneous sensing.[32,33]

iGr multifunctional sensors could offer promising solutions for wearable electronics, where flexible devices are required to ensure comfort when deployed on the human body. iGr offers a high sensitivity of electrical properties in response to external stimuli. Both, charge transport through individual graphene flakes and inter-flake charge transport are highly sensitive to T, P, RH etc. Of additional benefit is its thermal conductivity, mechanical flexibility, and biocompatibility compared to other 2D materials (e.g., hBN[34] or MoS_2[35]). The stable and reproducible performance of iGr films under bending cycles demonstrated here confirms that the devices can withstand the mechanical stress required for this application. Further work is needed to adjust the iGr ink formulation to achieve optimized performance under stretching. We note, that the composition and architecture of the device can be adjusted for the target application, for example, elastic dielectric polymers[36] can be used for enhanced performance under mechanical deformation. This will be beneficial for applications such as diagnostic and monitoring devices, applicable to a healthcare setting. Stimuli of interest (temperature, pressure and humidity) are largely in line with those presented here, as these offer significant relevance in a range of epidermal-level clinical settings ranging from wound healing monitoring to pressure ulcer pre-emption.[37] However, there are also a range of printed devices that could exploit the work undertaken here to sense a variety of parameters for various purposes, including pH,[38] lactate,[39] and electroactive analytes.[40]

The significant interest in inkjet printed graphene sensors is driven by advantageous and cost-effective fabrication approach, compared to the sensors fabricated using traditional methods such as chemical vapor deposition, mechanical exfoliation or spin coating.[41] The sensitivity of electrical properties of iGr, combined with design freedom offered by inkjet deposition make it a very promising materials for multifunctional sensors, especially for flexible and wearable substrates, which cannot be processed with conventional manufacturing technologies. Our sensor on fabric has a sensitivity of 1.45 kΩ $°C^{-1}$ for temperature sensing, a continues response to humidity from 35% to 100%, and sensitivity of 3.4kΩ kPa^{-1} for pressure sensing, We demonstrated multifunctional sensing capability on flexible substrate and on fabric, with performance better or comparable to that reported for single-function sensors.[42,43] Hence we propose that our technology offers beneficial solutions for multifunctional sensing.

3. Conclusion

In summary, a multifunctional graphene sensor was achieved in this work by exploiting inkjet printing of low dimensional and polymeric materials to produce device architectures with high degree of geometric freedom. Its functionality, sensitivity, and response time were tested in response to temperature, pressure and humidity, and demonstrated capability for simultaneous monitoring of several stimuli. The sensor was successfully inkjet printed on a variety of flexible and rigid substrates, such as Kapton tape, Si/SiO_2, glass, and fabrics. The sensitivity and performance of the sensor were found to be independent of the substrate used but highly dependent on the thickness of the deposited iGr layers. Droplet-printed devices demonstrated electronic properties different from those of iGr films, such as superlinear dependence of the device conductivity on the film thickness, high reproducibility of device conductivity, and strong gating effects. iGr films on Kapton and fabrics showed stable performance in response to environmental factors such as temperature, humidity and pressure. These findings open interesting prospects for the development of inkjet-printed multifunctional graphene sensors for applications including environmental monitoring, healthcare, and quantum technologies.

4. Experimental Section

Materials: Graphene ink (product number: 793663), tripropylene glycol diacrylate (TPGDA) monomer (product number: 246832), 2,4-diethyl-9H-thioxanthen-9-one (DETX, product number: 406368) and ethyl 4-dimethylamino benzoate (EDB, product number: E24905) were purchased from Merck. The graphene ink consisting of liquid exfoliated graphene

flakes (average size of 2590 nm^2) encapsulated in ethyl cellulose and dispersed into an 85:15 mixture of cyclohexanone/terpineol were further diluted to 2.4 solid wt.% to achieve suitable rheological properties for inkjet printing. The Ag nanoparticle ink was purchased from Advanced Nano Products (product ID: SilverJet DGP-40LT-15C) and consisted of 38.85 wt.% of silver nanoparticles dispersed in triethylene glycol monomethyl ether (TGME) and other dispersants. The Kapton film (536-3952) and PTFE tape (183-3490) were purchased from RS-Pro. The sapphire substrate was supplied by PI-KEM. The fabric used was a polyester cotton blend (65:35 respectively).

Inkjet Printing: Using Fujifilm DMP-2810 printer with DMC-11610 10pL cartridge, the top and bottom graphene tracks (1.2 cm × 0.12 cm) separated by 0.15 cm gap were printed using the graphene ink with a drop spacing of 10 µm and the number of layer N_L = 10,[36] and annealed at 250 °C in vacuum for 1 h. The dielectric separation layer consisting of 25 printed layers was printed using TPGDA monomer mixed with 8 wt.% photoinitiator (4 wt.% DETX and 4 wt.% EDB), with a drop spacing of 10 µm, and cured using in situ 365 nm UV LED during printing.[21] iGr droplet devices were produced with a few (1–5) droplets deposited directly on top of each other on a conventional Si/SiO_2 substrate with Ti/Au electrodes separated by 5–20 µm gap. To manufacture fabric-based iGr devices, 50 layers of TPGDA were first printed on the fabric (polyester-cotton with composition 65:35) and cured. A 50-layer graphene zigzag was then printed upon the TPGDA-fabric and consequently annealed in a 250 °C vacuum oven for 4 h.

Device Characterization: Electrical characterization was performed using a Keithley 2400 SourceMeter to simultaneously apply voltage and measure current through the iGr droplet, stripes and the sensor. In cases where a back gate voltage measurement was required, a second Keithley 2400 SourceMeter was used to apply the gate voltage. Typically, electrical measurements were performed either in a vacuum cryostat ($P \approx 10^{-6}$ mbar) or in a closed-cycle helium cooled cryostat (Cryogenics) for measurements in the temperature range 1.6 K < T < 400 K and magnetic field up to $B = \pm 16$ T. Humidity sensing was tested by putting the device in a sealed container with saturated salt solutions to control humidity environment ($MgCl_2$ for RH = 33%, K_2CO_3 for RH = 43%, $Mg(NO_3)_2$ for RH = 52%, NaCl for RH = 75.5%, KCl for RH = 86% and K_2SO_4 for RH = 97%). The relative humidity was monitored using a gyrometre in the container and I–V curve was measured when the humidity in the container was stable. The capacitance for pressure sensing was measured by a Rohde & Schwarz HM8018 LCR metre at 10 kHz and pressure was applied by putting a weight on a glass disc on top of the sensor.

Supporting Information

Supporting Information is available from the Wiley Online Library or from the author.

Acknowledgements

The authors acknowledge support from the Engineering and Physical Sciences Research Council [grant number EP/P031684/1, EP/W017032/1 and EP/T001046/1]; and University of Nottingham Propulsion Futures Beacon. The authors acknowledge Dr Jonathan H. Gosling and Mr Moises Clemente Guzmán for useful discussions, Dr Nicky Weston for assistance with ESEM and nmRC for access to analytical instrumentation.

Conflict of Interest

The authors declare no conflict of interest.

Data Availability Statement

The data that support the findings of this study are available from the corresponding author upon reasonable request.

Keywords

flexible electronics, graphene, inkjet deposition, multifunctional sensor, sensor

Received: August 30, 2024
Revised: October 23, 2024
Published online:

[1] S. Yao, P. Swetha, Y. Zhu, *Adv. Healthcare Mater.* **2018**, *7*, 1700889.
[2] M. F. Farooqui, M. A. Karimi, K. N. Salama, A. Shamim, *Adv. Mater. Technol.* **2017**, *2*, 1700051.
[3] K. S. Novoselov, A. K. Geim, S. V. Morozov, D.-e. Jiang, Y. Zhang, S. V. Dubonos, I. V. Grigorieva, A. A. Firsov, *Science* **2004**, *306*, 666.
[4] F. Koppens, T. Mueller, P. Avouris, A. Ferrari, M. S. Vitiello, M. Polini, *Nat. Nanotechnol.* **2014**, *9*, 780.
[5] F. Xia, T. Mueller, Y.-m. Lin, A. Valdes-Garcia, P. Avouris, *Nat. Nanotechnol.* **2009**, *4*, 839.
[6] C. Wang, K. Xia, H. Wang, X. Liang, Z. Yin, Y. Zhang, *Adv. Mater.* **2019**, *31*, 1801072.
[7] F. Schedin, A. K. Geim, S. V. Morozov, E. W. Hill, P. Blake, M. I. Katsnelson, K. S. Novoselov, *Nat. Mater.* **2007**, *6*, 652.
[8] Z. Wang, M. Shaygan, M. Otto, D. Schall, D. Neumaier, *Nanoscale* **2016**, *8*, 7683.
[9] J. N. Coleman, *Acc. Chem. Res.* **2013**, *46*, 14.
[10] D. Li, W. Y. Lai, Y. Z. Zhang, W. Huang, *Adv. Mater.* **2018**, *30*, 1704738.
[11] D. McManus, S. Vranic, F. Withers, V. Sanchez-Romaguera, M. Macucci, H. Yang, R. Sorrentino, K. Parvez, S.-K. Son, G. Iannaccone, *Nat. Nanotechnol.* **2017**, *12*, 343.
[12] F. Wang, J. H. Gosling, G. F. Trindade, G. A. Rance, O. Makarovsky, N. D. Cottam, Z. Kudrynskyi, A. G. Balanov, M. T. Greenaway, R. D. Wildman, *Adv. Funct. Mater.* **2021**, *31*, 2007478.
[13] T. Carey, S. Cacovich, G. Divitini, J. Ren, A. Mansouri, J. M. Kim, C. Wang, C. Ducati, R. Sordan, F. Torrisi, *Nat. Commun.* **2017**, *8*, 2.
[14] S. Barwich, J. M. de Araújo, A. Rafferty, C. G. da Rocha, M. S. Ferreira, J. N. Coleman, *Carbon* **2021**, *171*, 306.
[15] A. C. Neto, F. Guinea, N. M. Peres, K. S. Novoselov, A. K. Geim, *Rev. Mod. Phys.* **2009**, *81*, 109.
[16] J. Li, F. Ye, S. Vaziri, M. Muhammed, M. C. Lemme, M. Östling, *Adv. Mater* **2013**, *25*, 3985.
[17] V. Beedasy, P. J. Smith, *Materials* **2020**, *13*, 704.
[18] A. Bastola, Y. He, J. Im, G. Rivers, F. Wang, R. Worsley, J. S. Austin, O. Nelson-Dummett, R. D. Wildman, R. Hague, *Mater. Today Electronics* **2023**, *6*, 100058.
[19] E. B. Secor, P. L. Prabhumirashi, K. Puntambekar, M. L. Geier, M. C. Hersam, *J. Phys. Chem. Lett.* **2013**, *4*, 1347.
[20] H. Rokni, W. Lu, *Sci. Rep.* **2017**, *7*, 42821.
[21] Y. He, F. Zhang, E. Saleh, J. Vaithilingam, N. Aboulkhair, B. Begines, C. J. Tuck, R. J. Hague, I. A. Ashcroft, R. D. Wildman, *Addit. Manuf.* **2017**, *16*, 153.
[22] S. Borini, R. White, D. Wei, M. Astley, S. Haque, E. Spigone, N. Harris, J. Kivioja, T. Ryhänen, *ACS Nano* **2013**, *7*, 11166.
[23] S. Fan, F. Boey, M. Abadie, *Exp Polym Lett.* **2007**, *1*, 397.
[24] J. H. Gosling, S. V. Morozov, E. E. Vdovin, M. T. Greenaway, Y. N. Khanin, Z. Kudrynskyi, A. Patanè, L. Eaves, L. Turyanska, T. M. Fromhold, *Nanotechnology* **2023**, *34*, 125702.
[25] N. D. Cottam, F. Wang, J. S. Austin, C. J. Tuck, R. Hague, M. Fromhold, W. Escoffier, M. Goiran, M. Pierre, O. Makarovsky, *Small* **2024**, *20*, 2311416.
[26] G. Calabrese, L. Pimpolari, S. Conti, F. Mavier, S. Majee, R. Worsley, Z. Wang, F. Pieri, G. Basso, G. Pennelli, *Nanoscale* **2020**, *12*, 6708.

[27] A. Baker, J. Alexander-Webber, T. Altebaeumer, T. Janssen, A. Tzalenchuk, S. Lara-Avila, S. Kubatkin, R. Yakimova, C.-T. Lin, L.-J. Li, *Phys. Rev. B Condens. Matter Mater. Phys.* **2012**, *86*, 235441.
[28] K. S. Novoselov, Z.-f. Jiang, Y.-s. Zhang, S. Morozov, H. L. Stormer, U. Zeitler, J. Maan, G. Boebinger, P. Kim, A. K. Geim, *Science* **2007**, *315*, 1379.
[29] D. Dodoo-Arhin, R. C. Howe, G. Hu, Y. Zhang, P. Hiralal, A. Bello, G. Amaratunga, T. Hasan, *Carbon* **2016**, *105*, 33.
[30] S. Chung, K. Cho, T. Lee, *Adv. Sci.* **2019**, *6*, 1801445.
[31] R. Saint, W. Evans, Y. Zhou, T. Barrett, T. Fromhold, E. Saleh, I. Maskery, C. Tuck, R. Wildman, F. Oručević, *Sci. Rep.* **2018**, *8*, 8368.
[32] W. Huang, M. Yin, J. Xia, X. Zhang, *Trends Food Sci. Technol.* **2024**, *151*, 104646.
[33] W. Huang, J. Xia, B. Glamuzina, X. Zhang, *Comput. Electron. Agric.* **2024**, *219*, 108758.
[34] A. M. Joseph, B. Nagendra, E. Bhoje Gowd, K. P. Surendran, *ACS Omega* **2016**, *1*, 1220.
[35] J. Li, M. M. Naiini, S. Vaziri, M. C. Lemme, M. Östling, *Adv. Funct. Mater.* **2014**, *24*, 6524.
[36] A. Dadvand, J. Lu, C. Py, T.-Y. Chu, R. Movileanu, Y. Tao, *Org. Electron.* **2016**, *30*, 213.
[37] J. Strebeck, *AORN J.* **2007**, *86*, 677.
[38] T. Pandhi, C. Cornwell, K. Fujimoto, P. Barnes, J. Cox, H. Xiong, P. H. Davis, H. Subbaraman, J. E. Koehne, D. Estrada, *RSC Adv.* **2020**, *10*, 38205.
[39] K.-L. Tsou, K.-Y. Chen, Y.-D. Chou, Y.-T. Cheng, H.-E. Tsai, C.-K. Lee, *Talanta* **2022**, *249*, 123598.
[40] C. Sriprachuabwong, C. Karuwan, A. Wisitsorrat, D. Phokharatkul, T. Lomas, P. Sritongkham, A. Tuantranont, *J. Mater. Chem.* **2012**, *22*, 5478.
[41] J. Miao, T. Fan, *Carbon* **2023**, *202*, 495.
[42] S. Afroj, N. Karim, Z. Wang, S. Tan, P. He, M. Holwill, D. Ghazaryan, A. Fernando, K. S. Novoselov, *ACS Nano* **2019**, *13*, 3847.
[43] X. Wu, W. Zhao, J. Duan, Z. Qu, J. Wang, B. Zhang, *Mater. Lett.* **2022**, *326*, 132952.